DEVELOPMENT OF A HUMAN BODY FINITE ELEMENT MODEL FOR RESTRAINT SYSTEM R&D APPLICATIONS

Jay (Zhijijan) Zhao, Gopal Narwani

TAKATA – Automotive Systems Laboratory, Inc.

Paper Number 05-0399

ABSTRACT

A human body finite element model for an average adult male was developed. The model is based on the integration of finite element models of body regions of the thorax, abdomen, shoulder and head-neck, previously developed at Wayne State University. The model includes details of the human skeleton and major soft tissues in these body regions, including the skull, spinal column, neck muscles, joint ligaments, ribcage, clavicle and shoulder bones and joints, lungs, heart, aorta, vena cava, esophagus, liver, spleen, and kidneys, and various connective arteries and veins, and pelvis.

Extensive validations of the human body model have been made against Post Mortem Human Subjects (PMHS) responses for the frontal and side impacts, as well as belt and surrogate airbag loading under various conditions of fifteen sets of pendulum tests performed and published by various researchers. The force-deflection characteristics of shoulders, thorax, and the abdomen are in good agreement with the experimental data.

The model was further validated against the chest band data of belted PMHS 30mph sled test (NHTSA bio-mechanics database, test #2860). The model predicts the histories of chest deflections and shapes of the fourth and eight rib sections. Robustness study in sled test simulations was made. The model performed well under the impact severities of 15-35 MPH in frontal and side impacts.

Stress analysis was made on the clavicle under lateral pendulum impact, on the abdominal solid organs under rigid bar impacts, and on the chest ribs under the 30mph belted PMHS sled test. Comparisons of the analysis results with autopsy results showed that the model can estimate possible locations of the bone and organ failures, consistent with the experimental observations.

INTRODUCTION

Research and development of next generation advanced automotive restraint systems presents a unique set of challenges.

A recent survey by MLIT/JAMA/JARI on ITARDA Traffic Accident data in 2000 [1] showed that in Japan 76% of occupant fatalities were involved in frontal crashes, and 20% in side crashes. Among the frontal accidents head injuries accounted for 40% of the total fatalities, followed by chest injuries 25%, abdomen injures 11%, and neck injuries 7%. This survey also showed that belt usage reduced fatalities of occupants in all-direction auto accidents, but was not effective for reduction of the serious injury rates of occupants. In the United States also, similar trends of occupant fatality percentages classified by automobile accident types and injured body regions of occupant, have been reported in various publications by Mulligan et al. [2], Cavanaugh et al. [3], Elhagediab and Rouhana [4], and Lee and Yang [5], etc..

We studied the NASS/CDS database from 1993 to 1999. 59,426 cases of the thoracic and abdominal soft tissue injuries of occupants involved in the frontal accidents (PDOF=11–1 o'clock, AIS=2+) were analyzed. We found out that the unrestrained occupants had more organ injuries: about 72% for aorta, 52% for liver, 49% for spleen, 48% for kidneys, 47% for lungs, and 25% for heart, among all the cases. Comparatively, the percentages of organ injury in the total injured occupants restrained with seat belt only were: 17% for aorta, 40% for liver, 37% for spleen, 39% for kidneys, 32% for lungs, and 68% for heart. For the occupants restrained with both seatbelt and airbag the organ injury rates were, 5% for aorta, 8% for liver, 12% for spleen, 12% for kidneys, 11% for lungs, and 6% for heart. These findings tell us that the seatbelt combined with airbag provided better protection for occupants.

It is a challenge to develop safer and more advanced restraint systems, maximizing the protection performance for all the human body regions while to eliminate or to minimize their possible side effects, especially on the thoracic and abdominal organs. To optimize the restraint load distribution on the human body, particularly to properly distribute load through the shoulder and upper thorax of occupant, we need to better understand the shoulder's mechanical response and transmission of load to the thorax in frontal, oblique, and lateral impacts.

Protection of elderly people is expected to get increased attention in the next generation restraint system designs. The population continues to age worldwide. It was estimated that by 2030, 25% of the population will be age 65 or older [6]. Older people in general are more susceptible to injury, primarily thoracic injury, and that the morbidity, mortality, and treatment costs for a given injury are typically higher for old people. Kent et al. [7] found that the chest deflection threshold for rib fractures is strongly dependent on age. To better protect occupants of all age groups, especially elderly people, we should look to improve methods and tools for system performance evaluation.

The efficacy or performance of restraint systems is assessed using a variety of tools. Anthropomorphic test devices (ATDs), or dummies, are often used. ATDs are instrumented to measure various mechanical parameters, including accelerations at the center of gravity (CG) of head, chest, pelvis, chest deflection, and neck & femur forces etc. These mechanical parameters, or combinations thereof, correlated with presence of injury in similar cadaver tests to some extent, are used as "predictors" of injury risk. However, ATDs have certain limitations. The shoulder complex and the abdomen body parts of ATDs have poor biofidelity. ATDs have no or very limited capability for assessment of injury of the soft tissues (internal solid organs, ligaments, tendons, facet joint, etc.) in the human body. As supplemental tools, Post Mortem Human Subjects (PMHS) or animal tests may be performed to provide additional biomechanical information. Because these tests are very expensive, laborious, and have limited repeatability, they are not often used in laboratory for restraint systems evaluation.

Computer aided engineering (CAE) plays an important role in restraint systems R&D. Human body model emerges as an important tool for assessment of occupant injury and restraint system performance. Specifically, a well-developed human body model helps in understanding injury mechanisms of the bony skeleton and soft tissues/organs of the restrained occupant under complex loading conditions in laboratory and real car crashes. The human body model, by taking into account changes of the anatomical structures and material properties due to aging, can be used to study aging factors to help evaluate restraint concepts for elderly occupant protection. The sled test simulations using the human body model, combined with a few PMHS component tests, will play an important role in assessment of restraint system performance and side effects. These tasks are impossible or very difficult to be conducted by using the current ATDs.

With the rapid advances in computer technology, sophisticated finite-element models of the human body have been developed in recent years. There currently are few published human body models. However, all of them have some limitations for the system R&D applications to our knowledge. Toyota Central R&D Lab., Inc. has developed the Finite Element Model of the Total Human Model for Safety (THUMS-AM50 version 1.52) [8]. This model has detailed human skeleton structures. But the model treats the thoracic and abdominal soft tissues as lumped masses. The vertebrae were defined as rigid bodies. These modeling methods limited the model usage for injury estimation of the soft tissues and thoraco-lumbar spine. Ford Motor Company constructed a human body model for an average adult male and validated its thoracic impact responses against a few sets of PMHS tests [9]. This model includes details of the skeleton and major thoracic and abdominal solid organs. However, it is not clear from the paper [9] that how much details of the anatomical structures in the shoulder complex were modeled in this model and that how reliable it is applied in sled test simulation applications. The other mid-sized human male body models commercially available, have similar deficiencies.

During past decades Bioengineering Center of Wayne State University (WSU) has published a human thorax model [10], a human abdomen model [11], a human shoulder model [12], a human neck model [13], and a human head model [14, 15]. These models were validated to some extent against data obtained from the PMHS pendulum tests. We used these models extensively and concluded that development of a human body model based on integration of these body part models should meet our needs and expectations.

The purpose of this research was to develop a robust and reliable human body model for our restraint system R&D applications. The basis of this work were finite element models of the body regions of the thorax, abdomen, and shoulder, developed at WSU. In order to achieve our goal we have made great efforts on improvement of the modeling methods and integration to achieve computation robustness and efficiency, as well as its validations.

METHODS AND MODEL DESCRIPTION

Model Improvement and Description

The whole human body model numbering scheme was designed as follows:

The first two digits of nodes and elements (numbered in millions), parts and materials (numbered in thousands) coincide with the sequence number for the following eighteen body parts: 1-brain, 2-skull, 3-neck, 4-shoulders, 5-left arm, 6-right arm, 7-thoracic bony structures, 8-thoracic soft tissues, 9-aorta, 10-lumbar spine, 11-abdominal soft tissues, 12-pelvis, 13-left femur, 14-right femur, 15-left knee, 16-right knee, 17-left tibia & foot, and 18-right tibia & foot.

To obtain better quality of finite elements, the model were remeshed particularly for the bodies of the torso skin, the pelvis flesh, the kidneys and the renal artery and vein, the abdominal hollow organs walls, the shoulder scapula, the Supraspinatus and Infraspinatus muscles. All the interfaces between or among anatomical sub-structures, basically modeled as tied nodes or surfaces, were reorganized. All the interactions among the anatomical structures, modeled as interface contacts, were redefined. The detailed finite-element models for the body parts of head and neck, and the rigid body models for the lower extremities were integrated.

Our new 3D FE model of the human body represents an average adult male with weight of 75Kg. It contains about 45,656 solid elements, 52,565 shell elements and 268 1-D elements, with total about 80,000 nodes and 99,000 elements. The minimum element mesh size is about 1.3mm (in the aortic arch region). Figure 1 shows this model. A description of the model by body regions is given below.

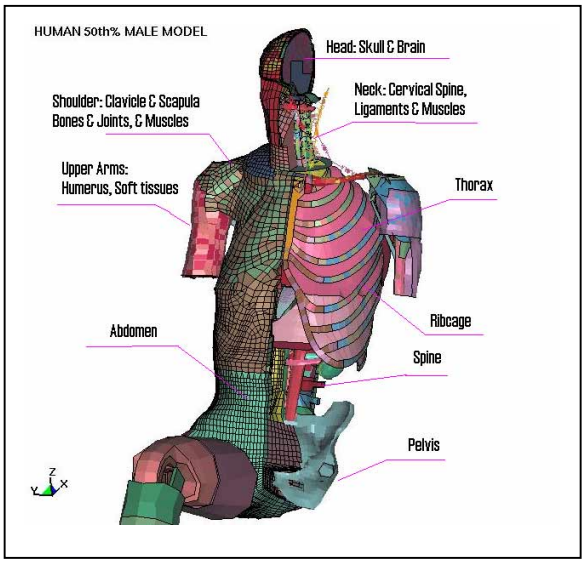

Figure 1. The human model model

The head model consists of scalp, skull, dura, falx, tentorium, venous sinuses, ventricles, cerebrum (gray and white matter), and cerebellum. The parts and material data are based on published information [14].

The neck model, consisting of the vertebrae from C1 through T1 including the intervertebral discs and anterior and posterior ligaments, synovial facet joints, and muscles, developed and validated against the data of PMHS free head-neck drop tests performed at Duke University [16] and PMHS pendulum rear impact to T1 conducted at WSU [13].

The shoulder model included three bones, the humerus, the scapula and the clavicle, and four joints, the glenohumeral, the acromioclavicular, the sternoclavicular joint, and the scapulothoracic articulation. Various muscles, tendons and ligaments in the shoulder complex are modeled. The modeling methods for the four joints were explained in the publication [12]. In this shoulder model, we redefined the bone-muscle-bone contacts for the Scapulo-thoracic Articulation and for the interactions between the ribcage and the posterior shoulder (Supraspinatus, Infraspinatus, Latissimus dorsi, Trapezius, and Deltoid) muscles. The material properties of the shoulder ligaments (those modeled as nonlinear elastic membrane) and muscles (those modeled as viscoelatic solid) were updated based on the latest experimental data from the dynamic loading tests for the human bone-ligament-bone

specimens of acromioclavicular, coracoclavicular and sternoclavicular joints [18].

The thorax model consists of the ribcage (spine, sternum, 12 pairs of ribs, and external and internal intercostals muscles) and internal soft tissues (heart, lungs, aorta, pleural, diaphragm, and the blood vessels and the air passages) [10]. In this model, the material model of the lungs is modeled using MAT_LUNG_TISSUE in the LS-DYNA code version 970 (LSTC, Livermore, California), in which the material coefficients were determined by fitting the experiment data of Michael Yen's bi-axial tests on excised specimens of human lung parenchyma [17]. The material model for the cortical bone (modeled as shell elements) and spongy bone (modeled as solid elements) uses elastic viscoplastic model combined with continuum damage mechanics (MAT_DAMAGE_2 in LS-DYNA). The intersection between parietal pleura and diaphragm was defined by tied-nodes. The left and right ventricles of the heart and the inside of the Aorta, Vena Cava and Esophagus were pressurized by airbag models.

The abdomen model contains the liver, spleen, kidneys, abdominal aorta, and inferior vena cava. A description of the original WSU abdomen model can be found in the paper [11]. Taking into considerations of better modeling of the anatomical interfaces among the solid and hollow organs and regional variation of the stiffness in between the midabdomen and the lower abdomen, we made some changes to the abdomen model. Instead of using one set of membrane elements to represent the whole cavity between the subcostal plane and the pelvic cavity [11], we defined a compressible solid in the cavity coupled with a set of membrane in a closed volume pressurized by an airbag. Additional arteries and veins (common iliac veins, external iliac artery, left and right renal veins, and veins and arteries connecting main vessels to the lumbar spine) were modeled. The density and the material properties of the liver, kidneys, and spleen were also updated based on the latest published experimental tests on the porcine liver, spleen and kidney specimens [19].

The thoraco-lumbar spine model is fully deformable. Twelve thoracic and five lumbar vertebrae were connected through discs and ligaments. We have conducted simulations using the sub-model of the lumbar spine to correlate the experimental data of the human cadaver lumbar tests under six different loading conditions of anterior and posterior shear, tension, compression, flexion and extension [20]. The responses of the lumbar spine model agree with the experimental data under all the loading conditions except for the flexion loading case. Adjustment of the material properties of the bones and ligaments of the spine was made.

The models for the lower extremity and lower arms and hands are relatively simple. The Hybrid-III legs were attached to the human body torso. To do so the pelvic bones of acetabulum and iliac were defined as rigid bodies. The anatomical data of the arms and hands were not included. Lumped mass were added to the upper arms to take into account their inertia effects.

Material Properties

Fourteen material models (constitutive laws) are used in the human body model. The material properties for some important tissues are listed in table A-1 in the appendix of this paper.

MODEL VALIDATION

PMHS Pendulum Impact Test Simulations

In our first round of the model validations, fifteen tests of PMHS pendulum impacts to three body regions of thorax, abdomen, and left shoulder were simulated. Table 1 summarizes the impact conditions and the sources of experimental data.

Thoracic Force-Deflection Responses

To validate the response of the thorax body region, five cases (case 1-5 as listed in Table 1) of the PMHS pendulum impact tests were simulated. The chest deflections were calculated from the displacement of the impact center point on the chest skin relative to the thoracic spine. In Cases 1-2, the forces were obtained from the anterior pendulum-body contact forces, while in Cases 3-5, the forces were from the posterior body-backplate contact. Comparisons of the force-deflection responses between the model and the test data are shown in Figures 1 to 5.

Table 1.

PMHS pendulum impact tests for the model validation

Case No.	Description of the test conditions	Ref. No.
1	23.4 Kg 150mm disk at 6.5 m/s to center of thorax	[21]
2	23.4kg 150mm disk 30 degree oblique impact to thorax at 6.5 m/s	[22]
3	UVA hub loading to thorax	[23]
4	UVA diagonal belt loading to thorax	[23]
5	UVA distributed loading to thorax	[23]
6	32Kg rigid bar impact to midabdomen at 6.1 m/s	[24]
7	48Kg rigid bar impact to midabdomen at 9.0 m/s	[25]
8	23.4kg disk 30 degree oblique impact to right side of upper abdomen at 6.5 m/s	[22]
9	Close-proximity surrogate airbag impact to midabdomen	[25]
10	Belt loading to midabdomen	[25]
11	23.4Kg disc lateral impact to left shoulder at 4.5 m/s	[12]
12	23Kg 200X150mm ram lateral impact to left shoulder at 4.4 m/s	[26]
13	The 23Kg ram 15 degree oblique impact to left shoulder at 4.4 m/s	[26]
14	The 23Kg ram 30 degree oblique impact to left shoulder at 4.4 m/s	[26]
15	The 23Kg ram 30 degree oblique impact to left shoulder at 7.6 m/s	[26]

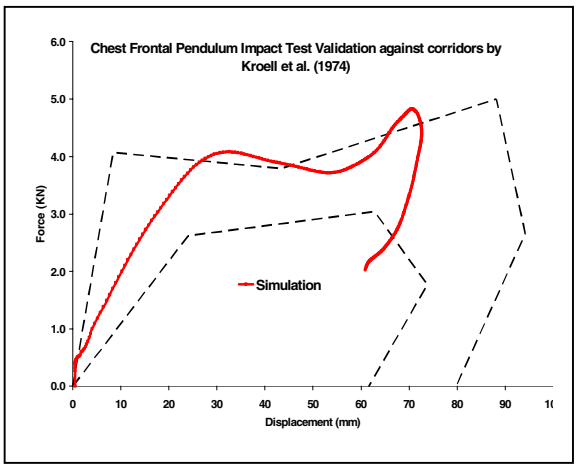

Fig.1 Force-deflection comparisons of Case 1

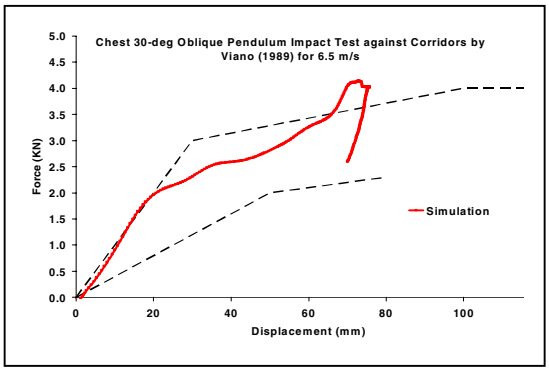

Fig. 2 Force-deflection comparisons of Case 2

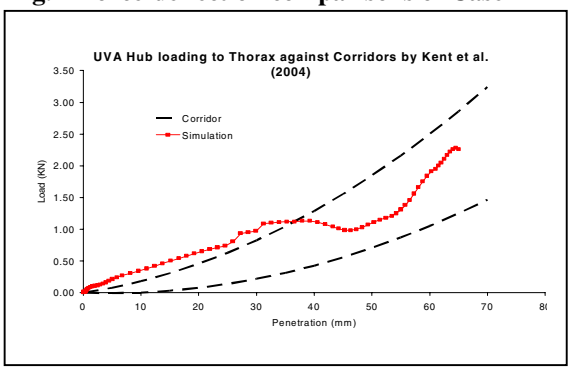

Fig. 3 Force-deflection comparisons of Case 3

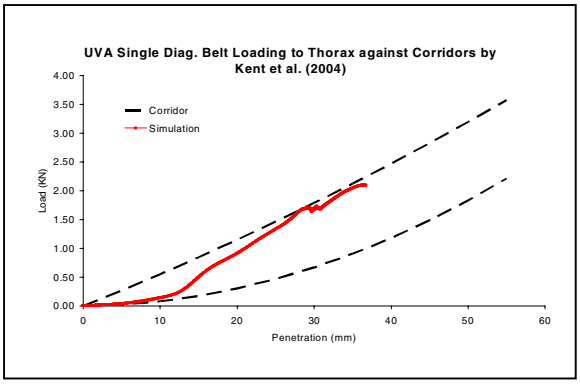

Fig.4 Force-deflection comparisons of Case 4

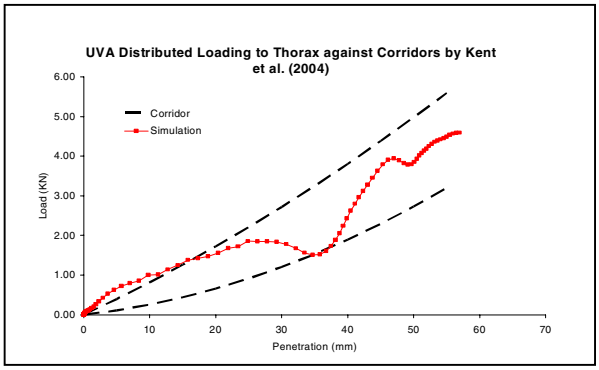

Fig.5 Force-deflection comparisons of Case 5

All these figures show that the calculated chest force-deflection responses are basically in the corridors of the test data by Kroell [21], Viano [22], and Kent et al. [23].

These results verified the model's predictions of the chest force-deflection responses to change of impact directions (cases 1 & 2) and types of loading (cases 3-5).

Abdominal Force-Deflection Responses

Cases 6 to 10 were set up to validate the model's abdominal responses to different impact mass and speed, loading type and impact directions. The abdominal deflections were calculated from the displacement of the impact center point on the abdomen skin relative to the lumbar spine.

Figure 6 to 10 show correlations between the calculated and measured forces-deflection responses of the midabdomen or the upper abdomen for cases 6-10. We see that overall the model predicts the abdominal responses reasonably.

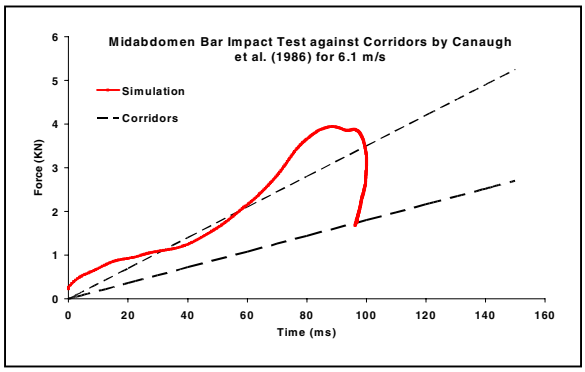

Fig. 6 Force-deflection comparisons of Case 6

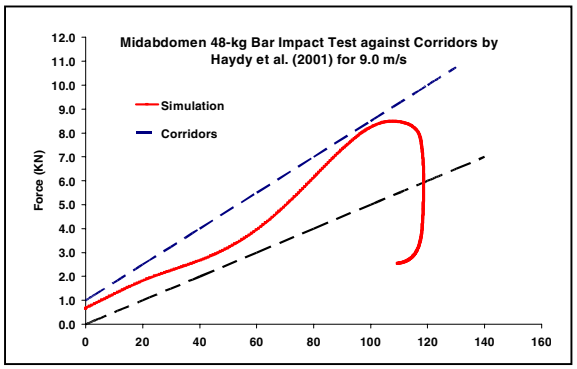

Fig. 7 Force-deflection comparisons of Case 7

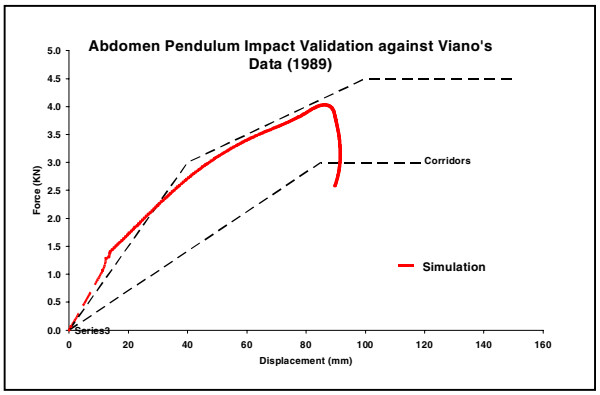

Fig. 8 Force-deflection comparisons of Case 8

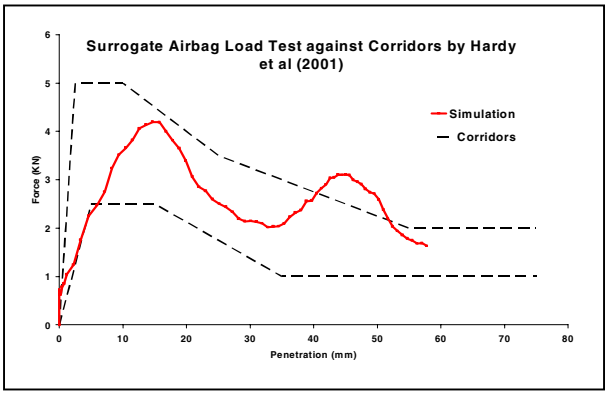

Fig. 9 Force-deflection comparisons of Case 9

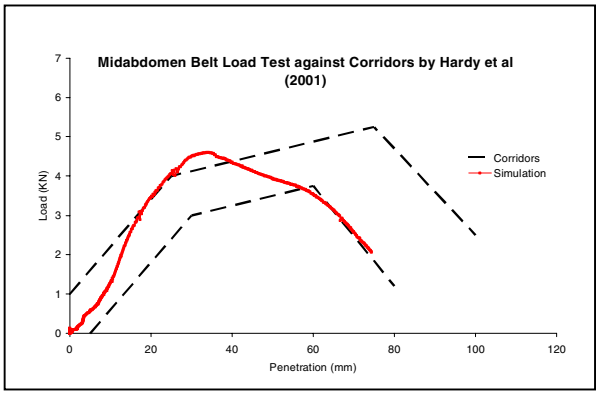

Fig. 10 Force-deflection comparisons of Case 10

Shoulder Force-Deflection Responses

Cases 11 to 15 were chosen to validate the responses of the shoulder. The shoulder deflections were calculated from the relative displacements of acromion-to-acromion. Comparisons of the forces-deflection responses between the model and the PMHS pendulum test data are shown in Figures 11 to 14. In the oblique impacts (Case 12-14), the responses in both y (the lateral direction) and x (the

anterior-posterior direction) were correlated with the data by Bolte et al [26].

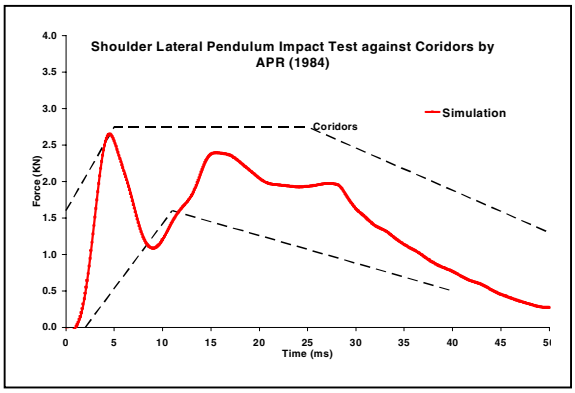

Fig. 11 Force-deflection comparisons of Case 11

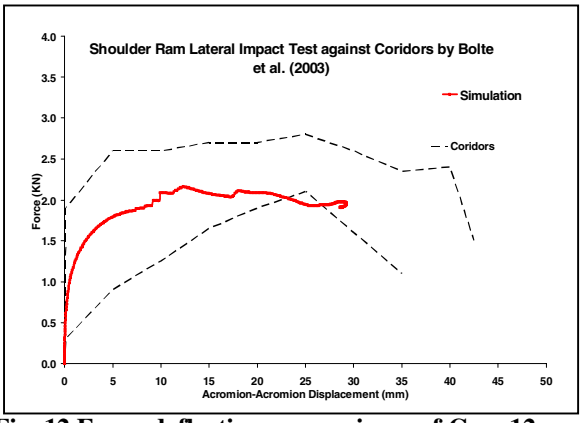

Fig. 12 Force-deflection comparisons of Case 12

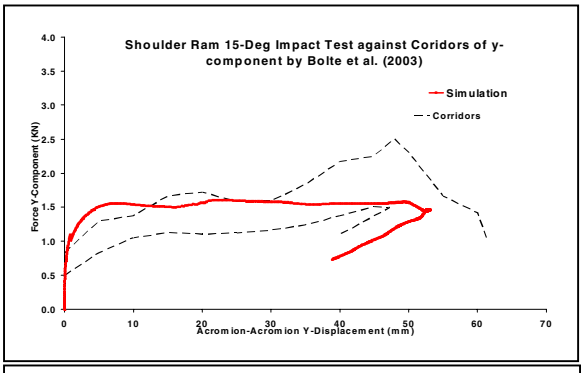

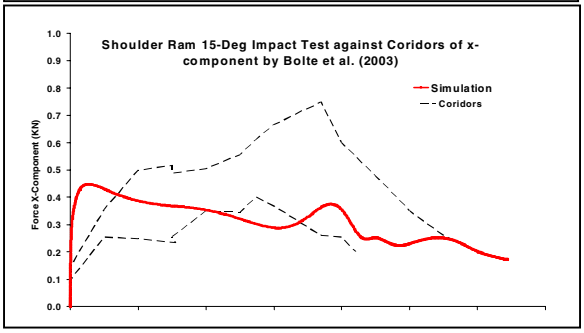

Fig. 13 Force-deflection comparisons of Case 13

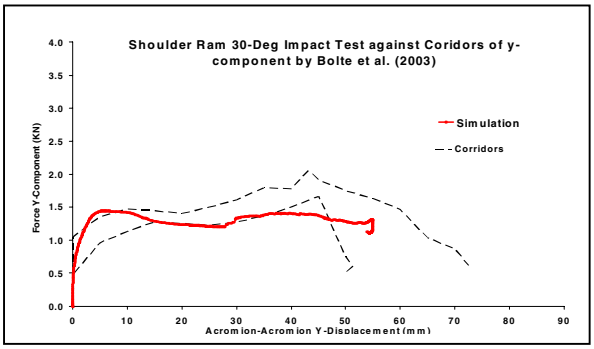

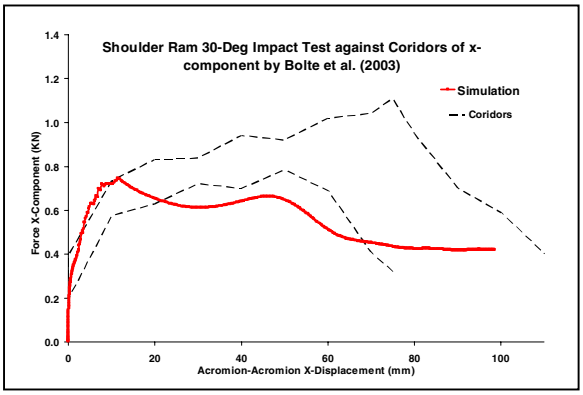

Fig. 14 Force-deflection comparisons of Case 14

PMHS Sled Test Simulation

For using the model as effective system evaluation tool, it is important to validate it under dynamic crash conditions. A set of PMHS sled test data in the NHTSA biomechanics database (test# 2860) was selected for such model validation. The test #2860 run at University of Virginia in 1992, used a 30.7 mph frontal crash pulse for a 3-point belted PMHS seated in a Tempo buck. The subject was an embalmed cadaver of 68 years old male with weight of 67Kg and height of 171cm. The test made use of two 40-gage chest bands, one on the fourth and one on the eighth rib to measure chest deformation during the impact event. The experimental data also included shoulder and lap belt forces, accelerations at T1 & T12 vertebrae and sternum.

The human body model was positioned in the test buck described in test report [27]. The belt system was modeled approximately in absence of details in the report. The sled crash pulse per this test report was used in the model.

The computed shoulder and lap belt forces were correlated with the test data. The model's predictions of the chest deflections were compared with available chest band measurement data.

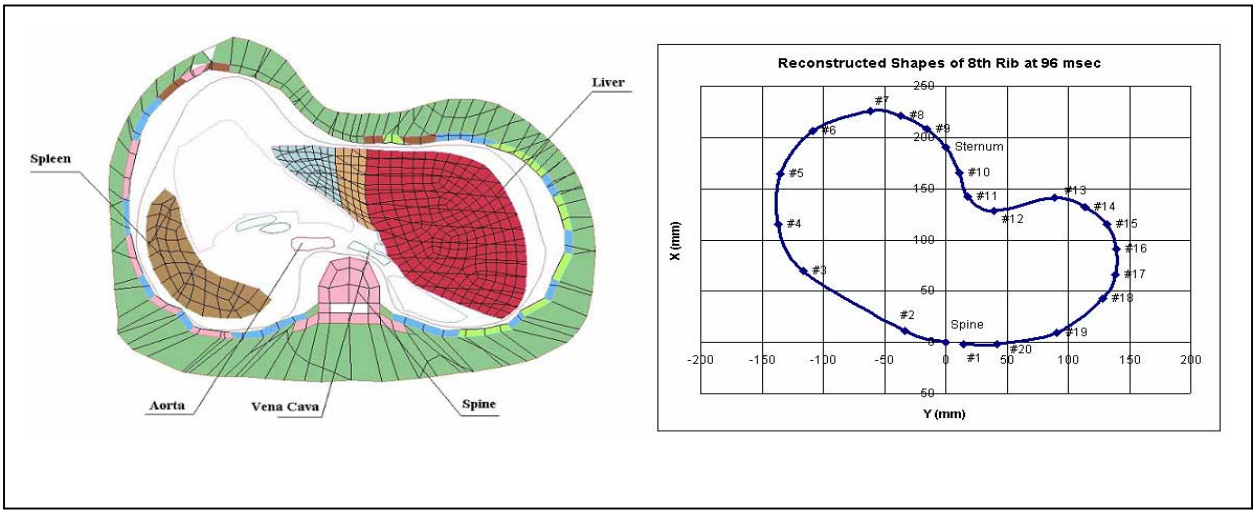

Fig. 17 Comparison between the simulated and experimental chest shapes at rib #8 at 96 msec

Figure 15 & 16 compare the model-predicted and measured histories of the chest deflections at rib #4 and #8 sections.

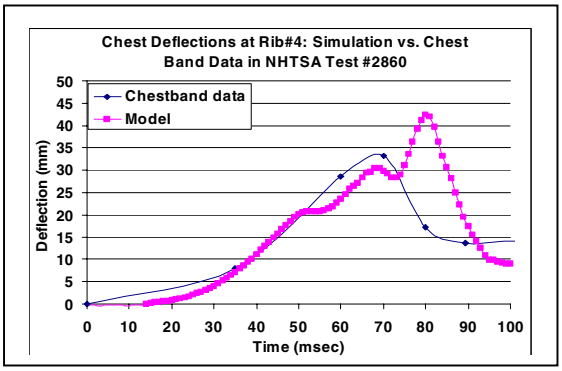

Fig. 15 Histories of the chest deflections at rib #4

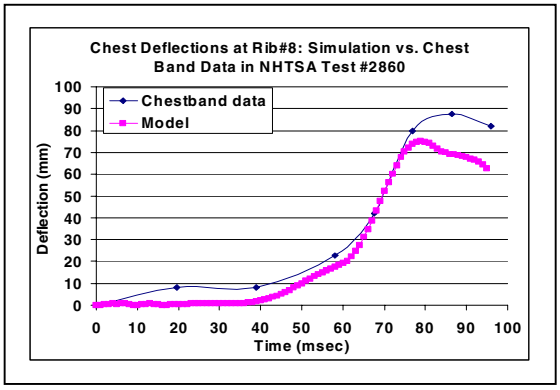

Fig. 16 Histories of the chest deflections at rib #8

The simulation results and the chestband data of chest deformation shapes within the time period of 120msec were also compared. Figure 17 shows such a comparison of the chest band shapes in the rib#8 transverse section plane at 96 msec. The computed profile is the transverse section view cut through the rib#8. The experimental shape was reconstructed from the chestband signals at 96 msec. The shapes are similar to each other.

These results give us some confidence in the human body model chest response estimations similar to PMHS under dynamic crash simulations.

Robustness Study in Sled Tests Simulations

To serve the needs of restraint system R&D applications, the human body model must be tested under various sled tests conditions. The motivation of this study was to assess robustness of the model in sled test simulations under a variety of restraint environments and crash conditions.

We set up a matrix that consisted of 12 runs, in which variations of crash severity (15 mph to 35 mph) and restraint systems (3-point & 4-point seatbelts, with or without driver & passenger airbags) were considered, as shown in Table 2.

All the simulations in the matrix were completed successfully. Robustness of such defined human sled test models was confirmed. Quantification of all of these model's results is in process.

Table 2.

Matrix of the human body sled tests for model robustness study

Run #	Occupant & Restraint Systems	Crash Pulse or Speed
1	Driver, 3pt-belted.	30mph
2	Driver, airbag only.	30mph
3	Driver, 3pt-belt + airbag.	35mph
4	Driver, 4pt-belt + airbag.	35mph
5	Driver, airbag only.	15mph
6	Passenger, 3pt-belted.	30mph
7	Passenger, airbag only.	30mph
8	Passenger, 3pt-belt +	35mph
9	Passenger, 4pt-belt +	35mph
10	Passenger, 3pt-belted.	15mph
11	WSU rigid wall side impact to a free occupant.	6.9 m/s
12	WSU rigid wall side impact to a free occupant.	9.1 m/s

INJURY ANALYSIS

Injury assessment and analyses were made for the simulation cases through the analysis of model predicted stress-strain field of hard and soft tissues in the shoulder, thorax and abdomen body regions. Comparing the injuries observed in the PMHS tests with model-predicted stresses should be helpful for us to understand the injury mechanism and to assess the model's capability and weakness for injury estimation at tissue level. In this section, the results of such analyses are presented.

Thoracic Rib Fracture Estimation

The sled test simulation case (NHTSA Test #2860 as analyzed above) was taken as a sample for this study.

The subject suffered multiple rib fractures in the sled test. In the right plot of Figure 18, white elliptic circles marks the approximate rib fracture locations reconstructed according to the published rib fracture report [27]. For comparison, the model-predicted stress contours of the ribcage at 100msec are shown in the left plot of Figure 18. We see that those high-stress areas concentrate around the observed fracture locations. The maximum Von Mises stresses of the ribs exceed 70MPa, while chest compression is more than 35%, indicating rib failures as compared the values (threshold of von Mises stress of 75-137 MPa) discussed in the publication [9].

Abdominal Organ Injury Estimation

Hardy's autopsy reports [25] of the rigid bar impacts to midabdomen of free-back cadavers were analyzed. Among the seven PMHS subjects under such test conditions five suffered liver injury and two had spleen injury. Table 3 summarized Hardy's findings particularly for the post-impact liver injuries.

Stress analysis was made on the liver based on the results of simulation case 7 from Table 1. Figure 19 gives anterior and posterior view of the Von Mises stress contours on the liver. We can see that in the high-stress concentrated areas the maximum Von Mises stresses are above 200KPa, exceeding the ultimate compressive stress thresholds in the range of 127-192 KPa [19]. These areas are most likely the origination of the tissue failures at those locations observed from the experiments described in Table 3.

Shoulder Injury Estimation

The tests data of ram impact to left shoulder of cadavers by Bolte [26] were analyzed. Among their fourteen tests reported, only one subject (Lat03) was found to have distal clavicle fracture. The test conditions were a lateral impact to the left shoulder of 84 years-old male subject of 64Kg weight at 4 m/s. The published radiograph showed the fracture location is on the clavicle close to Acronio-clavicular joint [26].

The model predicts the possible clavicle fracture locations which are in agreement with the experimental observation. As shown in Figure 20 left plot, the high-stress concentration areas are on the left clavicle around the Acronio-clavicular joint. The maximum Von Mises stresses of the clavicle are above 25 MPa..

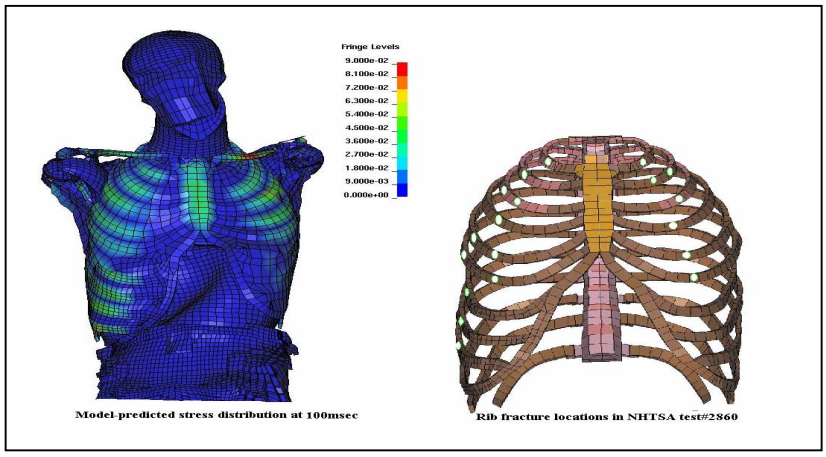

Fig. 18 Comparison between the simulated and experimental chest shapes at rib #8 at 96 msec

Table 3.

Hardy's autopsy results for liver injury from the cadavers subject to midabdomen rigid-bar impacts [25]

Test	Test Subject and Impact Speed	Liver Injury Description
GI1	Female, 73Y, 175cm, 36Kg. 4.3m/s.	NA
GI3	Male, 87Y, 173cm, 73Kg. 6.3m/s.	Vertical tear of right lobe, 7.5cm anteriorly, 9cm posteriorly.
GI4	Male, 93Y, 165cm, 58Kg. 6.6m/s.	Right capsule tear, 11cm anteriorly. Tear of left lobe, 3.5cm posteriorly.
GI6	Male, 85Y, 165cm, 91Kg. 6.1m/s.	Vertical tear of inferior edge, 2.5cm.
GI7	Male, 74Y, 181cm, 77Kg. 9.1m/s.	No liver injury.
GI8	Male, 71Y, 182cm, 64Kg. 9.0m/s.	Tear of inferior edge, 3cm. Multiple lacerations of left lobe posteriorly. Multiple lacerations of right lobe inferiorly.
GI9	Female, 85Y, 155cm, 51Kg. 9.6m/s.	Vertical tear of right lobe of liver, 5.0cm. Transverse tear of right lobe. Multiple irregular tears of right lobe posteriorly.

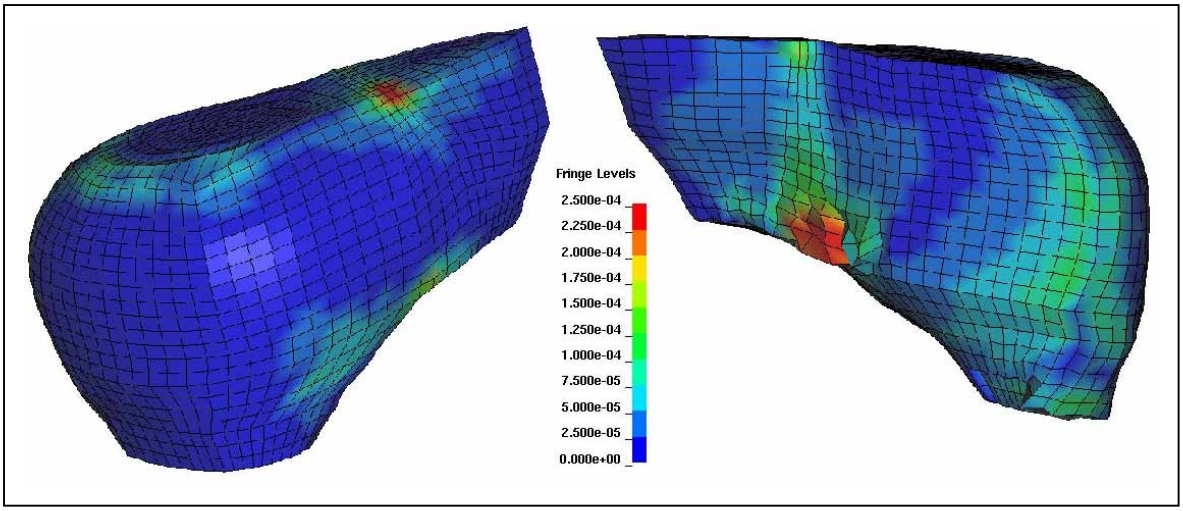

Fig. 19 Stress Contours of the liver at 48 msec at 9.0 m/s impact to midabdomen (simulation case 7)

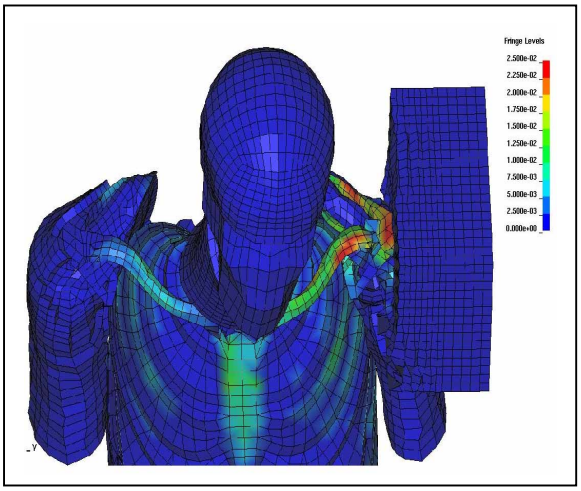

Fig. 20 Stress contours of the shoulders under ram impact at 4.4 m/s

CONCLUSIONS

A human body finite element model was developed for an average adult male with detailed bony and soft tissues in the body regions of the head-neck, shoulder, the thorax, and the abdomen.

Extensive validations of the human body model against Post Mortem Human Subjects (PMHS) responses for the frontal and side impacts, as well as belt and surrogate airbag loading under various conditions of fifteen sets of pendulum tests performed and published by various researchers were carried out. The force-deflection responses of shoulders, thorax, and the abdomen due to change of impact energy and directions, and types of loading are in good agreement with the experimental data.

This model was further validated against the chest band data of belted PMHS 30mph sled test. The model predicts the histories of chest deflections and deformed shapes of the fourth and eight rib sections. This study demonstrated that the model is applicable in sled test simulations under the impact severities of 15-35 MPH in frontal and side impacts.

Stress analysis made on the clavicle under lateral pendulum impact, on the abdominal solid organs under rigid bar impacts, and on the chest ribs under the 30mph belt PMHS sled test indicate that qualitatively this human body model can provide us very useful information about the possible failure locations of the skeletal and soft tissues in the body regions of the shoulder, the thorax and the abdomen under our considered loading conditions. However, accurate predictions of damage of the tissues are not possible by using the current model version. More work needs to be done both experimentally and analytically at the tissue level.

ACKNOWLEGEMENT

The authors would like to gratefully acknowledge Bioengineering Center of Wayne State University for providing us their base models for the development of finite element human body model reported in this paper. Special thanks to Dr. King Yang for his guidance and support for this research.

The authors also wish to acknowledge Dr. Jialou Hu at ASL/Takata for his helpful discussions regarding some material models.

REFERENCES

[1] MLIT/JAMA/JARI, "Proposals for Activities on International Harmonization Advanced Frontal Impact Dummies." IHRA BIO-WG in Washington D.C., USA, July 16, 2004.

[2] Mulligan, G.W.N., Pizey, G., Lane, D., Anderson, L., English, C., Kohut, C., "Thoracic Trauma Assessment Formulations for restrained Drivers In Simulated Frontal Impact." SAE Paper 942206, 1994.

[3] Cavanaugh, J., "The Biomechanics of Thoracic Trauma." In Accidental Injury Biomechanics and Prevention, Ed. By A. Nahum and J, Welvin, Springer-Verlag, New York, pp. 362-390, 1993.

[4] Elhagediab, A.M. and Rouhana, S.W., "Patterns of Abdominal Injury in Frontal Automotive Crashes." In Proceedings of the 16th International Technical Conference on Experimental Safety Vehicles, NHTSA, Washington D. C., Paper 98-S1-W-26, pp. 327-337, 1998.

[5] Lee, J.B. and Yang, K.H., "Abdominal Injury Patterns In Motor Vehicle Accidents: A Survey of NASS Database From 1993 to 1997, J. of Traffic injury Prevention, Vol. 3, No. 3, pp. 241-246, 2002.

[6] Kent, R., Sherwood, C., Lessley, D., Overby, B., Matsuoka, F., "Age-Related Changes In The Effective Stiffness of The Human Thorax Using Four Loading Conditions." in Proceedings of RCOBI Conference, 2003.

[7] Kent, R., Patrie, J., Matsuoka, F., Mullen, C., "Development of an Age-dependent Thoracic Injury Vriterion for Frontal Impact Restraint Loading." in

Proceedings of the 18th Technical Conference on the Enhanced Safety of Vehicles, Nagoya, Japan, 2003.

[8] Iwamoto M., Kisanuki Y., Watanable I., Furusu K., Miki K. and Hasegawa J., "Development of a Finite Element Model of the Total Human Model for Safety (THUMS) and application to injury construction, in Proceedings of IROCOBI, pp31-42, Munich, 2002.

[9] Ruan, J., El-Jawahri, R., Chai, L., Barbat, S., Prasad, P., "Prediction and Analysis of Human Thoracic Impact Responses and Injuries in Cadaver Impacts Using a Full Human Body Finite Element Model." Stapp Car Crash Journal, Vol. 47, Paper #2003-22-0014, 2003.

[10] Shah, C.S., Yang K., Hardy, W., Wang, H.K., King A.I., "Development of a Computer Model to Predict Aortic Rupture Due to Impact Loading." Stapp Car Crash Journal, Vol. 45, Paper #2001-22-0007, 2001.

[11] Lee, J.B. and Yang K., "Development of a Finite Element Model of Abdomen." Stapp Car Crash Journal, Vol. 45, Paper #2001-22-0004, 2001.

[12] Iwamoto, W., Miki, K., Mohammad, M., Naïf, A., Yang K., Begeman, P.C., and King, A.I., "Development of a Finite Element Model of the Human Shoulder." Stapp Car Crash Journal, Vol. 44, Paper #2000-01-SC19, 2000.

[13] Yang K., Zhu, F., Luan, F., Zhao, L., Begeman, P.C., "Development of a Finite Element Model of the Human Neck." Stapp Car Crash Journal, Vol. 42, Paper #983157, 1998.

[14] Zhou, C., Khalil, T.B., and King, A.I., "A New Model Comparing Impact Responses of the Homogeneous and Inhomogeneous Human Brain." Stapp Car Crash Journal, Vol. 39, Paper #952714, 1995.

[15] Zhang L., Yang K., Dwarampudi, R., Omori, K., Li, T., Chang K., hardy, W., Khaill, T.B. and King, A.I., "Recent Advances in Brain Injury Research: A New Human Head Model Development and Validation." Stapp Car Crash Journal, Vol. 45, Paper #2001-22-0017, 2001.

[16] Winkelstein, B.A., Nightingale, R.W., and Myers, B.S., "Impact Neck Injury Dynamics: Relationships between Impact Surface, Cervical Spine Kinetics, and Injury Risk." Proceedings of the 6th Injury Prevention through Biomechanics, pp. 85-95, 1996.

[17] Yen, Michael, R.T., "Development of Thorax Model Sub-project-C: Mechanical Properties of Human Heart, Lung and Aorta." Ph.D. Thesis of the Department of Biomedical Engineering of University of Memphis, September, 1999.

[18] Koh, S.W., Cavanaugh J.M., and Leach J.P., "Mechanical Properties of the Shoulder Ligaments under Dynamic Loading.", Stapp Car Crash Journal, Vol. 48, Paper #2004-22-0006, 2004.

[19] Tamura, A., Omori, K., Miki, K., Lee, B.J., Yang, K.H., King, A.I. "Mechanical Characterization of Porcine Organs.", Stapp Car Crash Journal, Vol. 46, Paper #2002-22-0003, 2002.

[20] Demetropouloa, C.K., Yang, K.H., Grimm, M.J., Khalil, T.B., and King, A.I. "Mechanical Properties of the Cadaveric and Hybrid III Lumbar Spines." Stapp Car Crash Journal, Vol. 42, Paper #983160, 1998.

[21] Kroell, C.K., Schneider, D.C. and Nahum, A.M., "Impact Tolerance and Response of the Human Thorax II." Stapp Car Crash Journal, Vol. 18, Paper #741187, 1974.

[22] Viano, D.C., "Biomechanical Responses and Injuries in Blunt lateral impact." Stapp Car Crash Journal, Vol. 33, Paper #8922432, 1989.

[23] Kent R. Lessley, D. and Shrewood, C., "Thoracic Response to Dynamic, Non-Impact Loading from a Hub, Distributed Belt, Diagonal Belt and Double Diagonal Belts." Stapp Car Crash Journal, Vol. 48, Paper #2004-22-0022, 2004.

[24] Cavanaugh, J.M., et al., "Lower Abdominal Tolerances and Responses." Stapp Car Crash Journal, Vol. 30, Paper #861878, 1986.

[25] Hardy, W., Schneider, W. and Rouhana, S.W., "Abdominal impact Response to Rigid-Bar, Seatbelt, and Airbag Loading." Stapp Car Crash Journal, Vol. 45, Paper #2001-22-0001, 2001.

[26] Bolte IV, J.H., Hines, M.H., Herriot, R.G., McFadden, J.D., and Donnelly, B.R., "Shoulder Impact Response and Injury Due to Lateral and Oblique Loading." Stapp Car Crash Journal, Vol. 47, Paper #2003-22-0003, 2003.

[27] Klopp G.S., "Test ASTS79, Using A Cadaver Utilizing A Three Point Seat Belt—A Report on a Test Run for NHTSA." Automobile Safety Laboratory of the University of Virginia, September 7, 1992.

APPENDIX

Table A-1.
Material properties for some important tissues

Tissues	Material Model	Density kg/m3	Young's Modulus(GPa)	Poison Ratio	Yield Stress (GPa)	Tangent Modulus (GPa)
Cervical vertebrae	Elastic	2500	0.354	0.3		
Cervical Intervertebral disc	Elastic-Plastic	1000	0.253	0.3	0.0014	0.00265
Face-neck skin	Viscous foam	1090	E1=0.02 N1=5.0 V2=55.0 E2=0 V2=1.2 PR=0.45			
Clavicle sponge bone	Elastic-plastic	1000	1.6	0.3	0.021	0.055
Clavicle cortical bone	Piecewise-plastic	2000	11	0.3	0.22	3.66
Clavicle cartilage	Elastic-plastic	1000	0.02071	0.45	0.0062	0.001
Clavicle cortical bone	Elastic-plastic	2000	11.5	0.3	0.123	4.17
Spongy bone for thoracic ribs	Damage_2	1000	0.04	0.45	0.0018	0.032
Coastal cartilage	Damage_2	1500	0.04901	0.4	0.00484	0.0156
Cortical bone for thoracic ribs	Plasticity with Damage	2000	10.18	0.3	0.0653	2.3
Rib cartilage	Elastic-plastic	1000	0.0227	0.35	0.0062	0.001
Costal muscle	Elastic-plastic	1000	0.0103	0.4	0.073	0.00103
Esophagus	Elastic	1200	0.005	0.4		
Lung	Lung Tissue	700	K=0.05, C=3.88E07, α=5.85, β=-3.21 C1=1.265E-8 C2=2.71 (in kg-mm-msec unit)			
Heart	Low Density Foam	1000	0.003	TC=0.01 HU=0.95 Loading/unloading compression function specified.		
Pulmonary trunk	Elastic	1200	0.005	0.4		
Pulmonary veins	Elastic	1200	0.01	0.4		
Mediastinal pleura	Elastic	1200	0.015	0.4		
Trachea	Elastic	1200	0.005	0.4		
Aorta	Elastic	1200	0.005	0.4		
Thoracic vertebrae	Elastic	2500	0.354	0.3		
Thoracic intervertebral disc	Elastic-plastic	1000	0.005	0.4	0.0014	0.00265
Lumbar vertebrae	Elastic	2500	0.354	0.3		
Lumbar disc	Elastic-plastic	1000	0.005	0.4	0.0014	0.00265
Spleen	Viscous Foam	1100	E1=4.88E-04 N1=4.0 V2=0.015 N2=0.2, E2=.025 N2=0.2 PR=0.45			
Kidney	Viscous Foam	1100	E1=0.0012 N1=5.0 V2=0.015, N2=0.2, E2=0.015 N2=0.2 PR=0.45			
Diaphragm	Elastic	1000	0.0655	0.4		
Lower abdomen Flesh	Elastic	1200	8.0E-04	0.4		